ACS APPLIED MATERIALS & INTERFACES

Research Article

www.acsami.org

Infrared-Actuated Recovery of Polyurethane Filled by Reduced Graphene Oxide/Carbon Nanotube Hybrids with High Energy Density

Yiyu Feng,[†] Mengmeng Qin,[†] Haiqiang Guo,[†] Katsumi Yoshino,[‡] and Wei Feng*,[†]

[†]School of Materials Science and Engineering, Tianjin University and Tianjin Key Laboratory of Composite and Functional Materials, Tianjin 300072, P. R. China

[‡]Shimane Institute for Industrial Technology, Hokuryo-cho, Mastue, Shimane 690-0816, Japan

Supporting Information

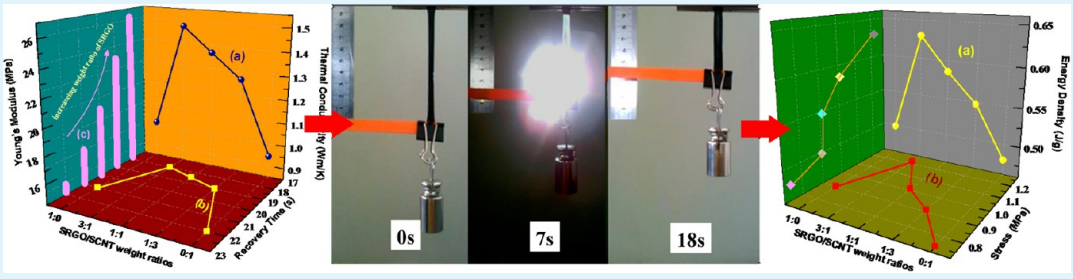

ABSTRACT: Optically actuated shape recovery materials receive much interest because of their great ability to control the creation of mechanical motion remotely and precisely. An infrared (IR) triggered actuator based on shape recovery was fabricated using polyurethane (TPU) incorporated by sulfonated reduced graphene oxide (SRGO)/sulfonated carbon nanotube (SCNT) hybrid nanofillers. Interconnected SRGO/SCNT hybrid nanofillers at a low weight loading of 1% dispersed in TPU showed good IR absorption and improved the crystallization of soft segments for a large shape deformation. The output force, energy density and recovery time of IR-triggered actuators were dependent on weight ratios of SRGO to SCNT (SRGO:SCNT). TPU nanocomposites filled by a hybrid nanofiller with SRGO:SCNT of 3:1 showed the maximum IR-actuated stress recovery of lifting a 107.6 g weight up 4.7 cm in 18 s. The stress recovery delivered a high energy density of 0.63 J/g and shape recovery force up to 1.2 MPa due to high thermal conductivity (1.473 W/mK) and Young's modulus of 23.4 MPa. Results indicate that a trade-off between the stiffness and efficient heat transfer controlled by synergistic effect between SRGO and SCNT is critical for high mechanical power output of IR-triggered actuators. IR-actuated shape recovery of SRGO/SCNT/TPU nanocomposites combining high energy density and output forces can be further developed for advanced optomechanical systems.

KEYWORDS: *infrared actuators, reduced graphene oxide, shape recovery, high density, carbon nanotube*

1. INTRODUCTION

Stimulus-responsive shape memory materials (SMM) are able to recover a significant deformation from a temporary large-scale shape actuated by different external stimuli including heat, stress, current/voltage, light, magnetic, and pH/moisture/chemicals.[1,2] This intriguing shape recovery enables SMM to have the ability to control the creation of mechanical motion rapidly and precisely. Therefore, a variety of actuators using SMM is fabricated for many applications ranging molecular switches, oscillators to adaptive biomedicals,[3−5] in which an effective "trigger" is capable of releasing the strain stored in metastable structures resulting from the crystallization, cross-linking, orientation, isomerization or chemical reaction through a large shape recovery. However, a majority of these actuators is driven by external electric power, magnetic field, specific chemical compounds, or heat sources.[6−8] In contrast, light or laser, especially infrared (IR) light with wide emission and heat radiation effect, has catalyzed a growing interest in the use as a triggering energy input because of its clear, enormous, and renewable nature. Optical actuators offer many distinctive advantages over other switches such as a high level of integrity, remote or wireless control, good scalability and adaptability in harsh environment.[9] Furthermore, optically triggered shape recovery of SMM can be further improved by optimizing the absorption of wavelength-specific photon, thermal conduction, and mechanical properties.

Significant progresses on optical actuators based on shape recovery of functional polymers have been made for many technological uses, including optomechanical systems for high-precision waveguide, light-driven oscillator, and microrobots, because of their light weight, flexible processability, low recovery temperature, and tailorable properties.[10−12] Many

Received: July 28, 2013
Accepted: October 2, 2013
Published: October 2, 2013

conductive and strong nanofillers or nanoparticles have been used to improve energy transfer and mechanical strength of polymers. The output force and energy density of shape recovery of polymer nanocomposites are mainly determined by mechanical properties, optical absorbance and heat conduction of inter- or intermolecular fillers. However, optomechanical stress (forces) output from a large reversible shape recovery is still much lower than the requirement of a device-level output force of actual actuators.[9,10,13] Moreover, energy density and power conversion efficiency, resulting from stress, strain, and recovery time, are also rather low. To date, combining large stress and strain recovery, as well as high energy density, remains a significant challenge for optically active shape memory polymer nanocomposites.[9]

Carbon nanostructures, as well as nanospheres, nanotubes and nanosheets are regarded to be ideal nanofillers for optically actuated shape memory polymers due to their excellent thermal and mechanical properties at a quite low weight quantity (0.05−1%).[14−19] Vaia groups reported that one-dimensional (1D) multi-walled carbon nanotubes (MWCNT)/polyurethane (TPU) nanocomposite films hoisted a 60 g weight up 3.3 cm by a large-scale shape recovery upon remote IR irradiation, showing an energy density of ∼0.2 J/g.[15] However, this actuation performance relying on the structural uniformity, dispersion and high purity of CNTs are affected by surface defects, large bundles, impurities, the anisotropy and a structural mixture.[20] This problem can be partly overcome by using 2D graphene nanofillers with a perfect sp^2 carbon aromatic network. However, well-dispersed graphene in polymers is prepared by the surface functionalization, which results in the decrease in thermal conductivity due to structural defects.[21,22] Therefore, a balance between the restoration of aromatic network and the dispersion of graphene is crucial for the reinforcement and high thermal conductivity. Recently, a 3D interconnected network of graphene/CNT hybrid has been integrated into polymers as thermally conductive and strong nanofiller. Theoretical calculation and experimental measurement indicate that enhanced thermal conductivity and high mechanical strength of polymer nanocomposites using hybrid nanofiller are dependent on synergistic effect between well-dispersed graphene and CNTs, which also can be tuned by weight ratio of graphene to CNT.[23−27] Despite good thermal and mechanical properties, studies on optically triggered shape recovery of graphene/CNT-based polymers controlled by synergistic effect have been rarely reported.

In this paper, sulfonated reduced graphene oxide/carbon nanotube hybrid (SRGO/SCNT) nanofillers were utilized in TPU for the improvement of IR-triggered shape recovery. Well-dispersed SRGO/SCNT nanofillers were observed by transmission electron microscope (TEM). Optical absorbance and the crystallite structure of soft segments were characterized by NIR absorption spectra and differential scanning calorimetry (DSC), respectively. IR-triggered stress recovery of SRGO/SCNT/TPU nanocomposites including shape recovery force, energy density and recovery time with different weigh ratios of SRGO to SCNT (SRGO:SCNT) was studied. When SRGO:SCNT is 3:1, SRGO/SCNT/TPU nanocomposite delivered a energy density of 0.63 J/g and the output stress of 1.2 MPa due to efficient heat transfer and high mechanical strength controlled by synergistic effect between SRGO and SCNT.

2. EXPERIMENTAL SECTION

2.1. Raw Materials. Graphene oxide (GO) was prepared from natural foliate graphite by the modified Hummer's method. Raw MWCNT (the average diameter of 10-20 nm and the length of 30-70 μm) were purchased from Beijing DK nanotechnology Co. LTD. Raw samples were further purified by H_2O_2 at room temperature for one week to remove carbon and metal impurities.[28] TPU (Irogran PS455-200) was provided by Huntsman Polyurethanes. This linear segmented TPU shows a soft-segment crystalline at 38.1°C and hard-segment melting at ∼140 °C determined by DSC.

2.2. Synthesis of SRGO and SCNT. SRGO was prepared using diazotization reaction according to the literatures.[29] A typical preparation process contained three steps, partial reduction, diazotization reaction, and further restoration of aromatic structures: (1) GO (100 mg) was dispersed in 100 mL di-water by ultrasonication for 1 h, and then pH of solution was adjusted to 9 using 5 wt % $NaCO_3$ solution. 20 mL $NaBH_4$ aqueous solution (0.04 mg/mL) was added in GO solution, and the reduction was carried out at 80°C for 1 h. After washing with di-water for several times by filtration, partially reduced GO (RGO) was redispersed in 100 mL of di-water by ultrasonication for 1 h. (2) The diazonium salt was prepared using sulfanilic acid (184 mg) and $NaNO_2$ (72 mg) in 40 mL of di-water and 2 mL of HCl (1M) solution in an ice bath. This diazonium salt solution was added dropwise in 100 mL of RGO solution in an ice bath, and the reaction was carried out for 4 h at 0°C and another 2 h at room temperature. SRGO was gained after washing with di-water for several times by filtration. 3) Well-dispersed SRGO in 100 mL di-water was further reduced using 6 mL of hydrazine hydrate (80%) at 100 °C for 24 h to remove many oxygen groups. The resultant SRGO was acquired after washing with di-water repeatedly until pH of SRGO solution was 7.

SCNT was also prepared using diazotization reaction. Purified MWCNT (200 mg) was added in the mixture (30 mL) of sulfuric acids and nitric acids (the mass ratio is 3: 1) by ultrasonication, and the mixure was heated at 50 °C for 2 h. Acid-treated MWCNT (100 mg) was obtained by centrifugation following by rinsing with di-water for several times until pH of solution was 7. SCNT was prepared using diazonium salt by the the same method to the second step of the synthesis of SRGO.

2.3. Synthesis of SRGO/SCNT/TPU Nanocomposite. SRGO/SCNT/TPU nanocomposite films were prepared by a solution-processed mixing method.[14,27,30] Briefly, SRGO/SCNT hybrid (10 mg) with different weight ratios were well-dispersed in 10 mL of dimethylformamide (DMF) by ultrasonication for 4 h to form a homogenous suspension. TPU (990 mg) was dissolved in 10 mL DMF at 70 °C. After cooling down to room temperature, TPU solution was slowly added in SRGO/SCNT solution in DMF under constant stirring. The mixture was further ultrasonicated for 1 h and immediately poured into a Teflon Petri dish for the formation of nanocomposite films. After the evaporation of solvents, these yielding films were peeled off for further testing. The total loading of hybrid nanofillers is 1 wt % in TPU matrix, and TPU nanocomposite films with SRGO:SCNT of 1:0, 3:1, 1:1, 1:3, and 0:1 (defined as SRGO, $SRGO/SCNT_{3:1}$, $SRGO/SCNT_{1:1}$, $SRGO/SCNT_{1:3}$, and SCNT) were used to study IR-triggered shape recovery.

2.4. Characterization. The morphologies of SRGO/SCNT nanofillers in TPU were observed by scanning electron microscopy (SEM, Hitachi S-4800) and high-resolution transmission electron microscopy (TEM, Tecnai G2 F20). SEM samples were fractured after immersing films in liquid nitrogen for 5 min and coated by gold particles. TEM samples with the thickness of about 100 nm were cut from the composite disks using the microtome. Chemical structures of TPU nanocomposites were charaterized by fourier transform infrared spectrometer (FT-IR, (Bruker Tensor 27, using KBr pellets). Vis-NIR absorption spectra were recorded using a JASCO V-570 spectrometer. Thermal conductivity of nanocomposite films was measured using DRX-II-RL Thermal Conductivity Meter. Thermal stability of soft and hard segments of TPU nanocomposites was recorded by DSC (Perkin-Elmer DSC-7) from 30 °C to 700 °C at a rate of 5 °C/min in an

aluminum crucible under 50 mL/min of nitrogen purging. Mechanical properties of TPU nanocomposite sample (~30 mm × 10 mm × 0.1 mm) were measured by a universal tensile testing machine (M350-20K, United Kingdom). The load cell was 100 N with a gauge length of 30 mm and the extension rate was kept at 20 mm/min. In all cases, more than five samples were tested, from which the mean and standard deviation were also calculated.

2.5. IR-Triggered Stress Recovery. Before the exposure to IR light, all samples were elongated by 250% of the original length at room temperature for strain-induced crystallization of soft segment. This enormous tensile deformation increases the density of physical cross-linking. To avoid the influence of thermomechanical history and crystallite distribution,[31] all samples were heated to relax the temporary elongated shape at ~70 °C for 5 min before the first shape recovery.[14] A xenon lamp at 500 W with a red filter set of >900 nm was positioned at 30 cm from the sample. The power density to nanocomposite film was ~30 mW/cm^2 measured by a light density meter (Beijing Zhongjiaojinyuan Co., Ltd.) Both ends of samples were fixed by specimen clamps. Stress recovery was measured by applying IR radiation to fixed samples for several seconds under the load of a total weight of ~107.5 ± 0.2 g. The process was recorded by a digital camera (SONY). Shape recovery force was recorded using a load cell in tensile force measurement[17] under the same IR radiation. The recovery shows a slight decrease exposed by IR light for a long time.

The performance of IR-triggered recovery such as the maximum recovery stress (σ_{max}), energy density (ω), and the percent recovery was calculated using following eqs 1−3:

$$\omega = \frac{G\Delta S}{m} \quad (1)$$

$$\sigma_{max} = \frac{F_r}{A_s} \quad (2)$$

$$\text{percent recovery} = \frac{\varepsilon_0 - \varepsilon_r}{\varepsilon_0} \quad (3)$$

where G is the total weight of loading, ΔS is the vertical displacement of loading, and m is the mass of the sample covered by IR light. F_r is the shape recovery force, A_s is the cross-section area of the prestrained sample, ε_0 is the prestrain of the sample, and ε_r is the retention shape after the recovery. Power conversion efficiency of IR-actuated recovery can also be estimated by the eq 4, where W_{out} is the mechanical energy output, W_{in} is the energy delivered by IR light, P_{IR} is the power density of IR light delivered on the sample, A_i is the surface area of sample covered by IR light, and t is the shape recovery time.

$$\eta = \frac{W_{out}}{W_{in}} = \frac{G\Delta S}{P_{IR}A_i t} \quad (4)$$

3. RESULTS AND DISCUSSION

Previous studies showed that the improvement of thermal and mechanical properties of graphene (CNT)-based polymers relied on the integrity of carbon conjugated structures and the dispersion of nanofillers.[14,19,32,33] The surface modification is an effective method to improve the interaction and compatibility between graphene (CNT) and polymers. Figure 1s in the Supporting Information shows that SRGO preserves a typical crumpling and silky morphology with the size of ~3 × 5 μm and SCNT exhibits a 1D tube structure with the diameter about 10−12 nm. Nanosheets and nanotubes are dispersed due to reduced van de Waals attraction by chemical groups such as $-SO_3H$ on the boundaries and sidewalls. The microstructures of SRGO/SCNT nanofillers in TPU were observed by SEM. The fracture surfaces of SRGO/TPU (Figure 1a) and SCNT/TPU (Figure 1b) show that nanoplatelets and nanotubes are dispersed uniformly in TPU. Furthermore, nanosheets (red square) and debundled tubes (blue circle) are also observed in the fracture section of SRGO/SCNT/TPU films (Figure 1c, d), indicating good compatibility between hybrid nanofillers and TPU.[19,23] The dispersion of SRGO/SCNT nanofillers was further observed by TEM (Figure 2). Well-dispersion of individual SCNT and SRGO in TPU matrix was shown in images a and b in Figure 2, respectively. Furthermore, a 3D interconnected network of SRGO/SCNT forms in polymers, in which 1D nanotubes as a bridge connect 2D nanosheets platforms. The interfacial connection between SRGO and SCNT (indicated by brown circles) favors efficient heat transfer and conduction through the nanofillers due to synergistic effect between SRGO and SCNT.[23,25] Besides, FT-IR spectra (see Figure 2s in the Supporting Information) show that chemical structures of TPU polymers were not changed by the integration of SRGO/SCNT hybrid except for a shift of the peak (from 1736 cm^{-1} of TPU to 1726 cm^{-1} of SRGO/SCNT/TPU) corresponding to −C═O− groups. This shift suggests the strong interaction between nanofillers and TPU with the formation of hydrogen bonds between hard segments and SRGO/SCNT.[17,20]

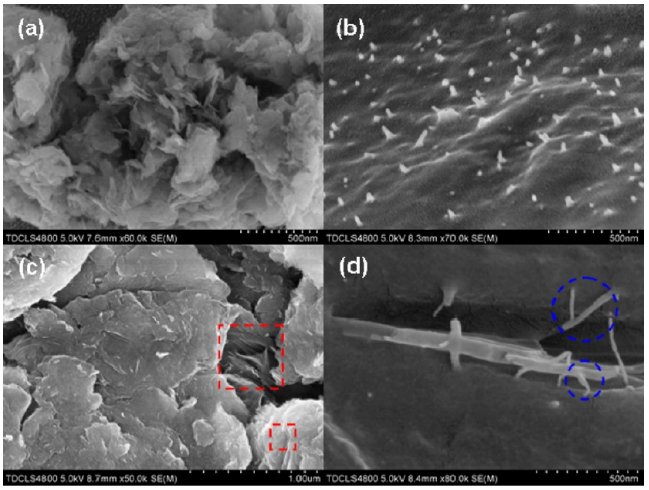

Figure 1. SEM images of TPU films incorporated by (a) SRGO, (b) SCNT, and (c) SRGO/SCNT nanofillers (d) at the cross-section.

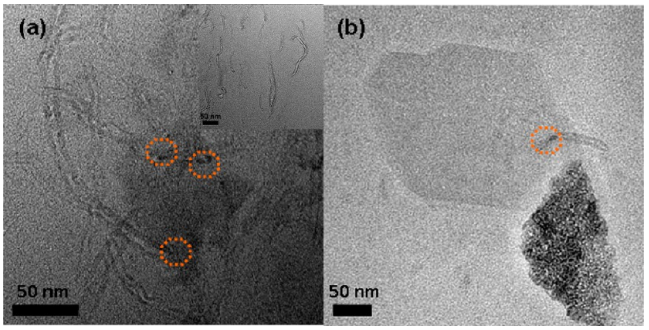

Figure 2. TEM images of SRGO/SCNT nanofillers in TPU matrix with the inset of well-dispersed SCNT.

Vis−NIR absorption spectra of SRGO/SCNT/TPU films with different weight ratios were given in Figure 3. Pure TPU film is nearly light transparent and shows weak absorption in vis−NIR region. SRGO/SCNT/TPU films exhibit a dramatic increase in IR absorbance in the range of 1100−650 nm due to the coupling of electronic states in the asymmetric stretch mode by oxygen groups at the defects of the edge of SRGO[34]

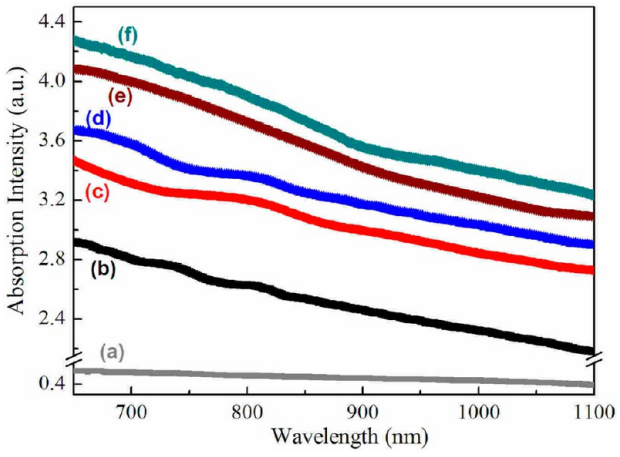

Figure 3. Vis–NIR Absorption spectra of (a) TPU, (b) SRGO/TPU, (c) SRGO/SCNT$_{3:1}$/TPU, (d) SRGO/SCNT$_{1:1}$/TPU, (e) SRGO/SCNT$_{1:3}$/TPU, and (f) SCNT/TPU films.

and on the sidewall of SCNT. Increasing IR absorption baseline of SRGO/SCNT/TPU films was also confirmed by the absorption spectra of SRGO/SCNT/TPU in DMF solution (see Figure 3s in the Supporting Information).[14,16] Moreover, curves also show a continuous increase in IR absorbance with a decreasing content of SRGO. This feature reveals that SRGO has less oxygen defects and shows lower dispersibility than SCNT due to partial restoration of conjugated structures.[34,35] IR absorption of SRGO/SCNT/TPU nanocomposite film is much higher than previous TPU/graphene,[14] indicating a good capability for light coupling. High IR absorbance controlled by the defects and uniform dispersion of SRGO/SCNT nanofillers[14,19,36] is basically important for IR-triggered shape recovery.

Thermal stability of segment crystallites of TPU was studied by DSC (Figure 4). Pristine TPU (Figure 4a) shows a typical characteristic endotherm peak at 38.1°, which is the melting point of soft-segment crystallites (T_{soft}), and a weak broad band at around 140° ascribed to the melting of crystallized parts of hard segments. DSC curves (Figure 4b–d) show that T_{soft} shifts

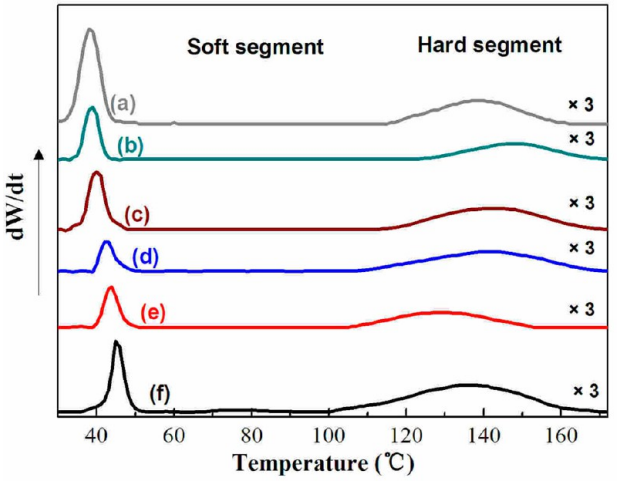

Figure 4. DSC curves of (a) TPU, (b) SCNT/TPU, (c) SRGO/SCNT1:3/TPU, (d) SRGO/SCNT1:1/TPU, (e) SRGO/SCNT3:1/TPU, and (f) SRGO/TPU film showing two endotherm bands due to the melting of soft and hard segments.

to high temperature by the incorporation of SRGO/SCNT hybrid. Moreover, SRGO/SCNT/TPU nanocomposites exhibit a continuous increase in T_{soft} with an increasing content of SRGO in hybrid nanofillers. Specifically, T_{soft} of TPU incorporated by SCNT, SRGO/SCNT$_{3:1}$, SRGO/SCNT$_{1:1}$, SRGO/SCNT$_{1:3}$, and SRGO nanofillers are 38.9, 39.0, 42.4, 43.8, and 45.5°C.

According to previous studies, enhanced thermal stability of soft segments arose from the heterogeneous nucleating effect of SRGO and SCNT in polymers.[37,38] Thus, the increase in T_{soft} indicates a good chemical affinity and interaction between nanofillers and TPU. Figure 4 displays that the crystallinity of soft segments is further improved with an increasing content of SRGO due to 2D planar structures. Enhanced soft-segment crystallinity of SRGO/SCNT/TPU nanocomposites not only increases storage capacity of strain-induced energy but also determines the temperature for IR-triggered shape recovery. Besides, there are no large shifts in melting temperature of hard segments, which is consistent with previous results of TPU with a low weight loading of carbon nanofillers.[14,15,39] Results suggest that SRGO/SCNT nanofillers have little impact on regular ordered crystallized structures of hard segments.

IR-actuated shape recovery of SRGO/SCNT/TPU nanocomposite films are illustrated in Figure 5a. Before the

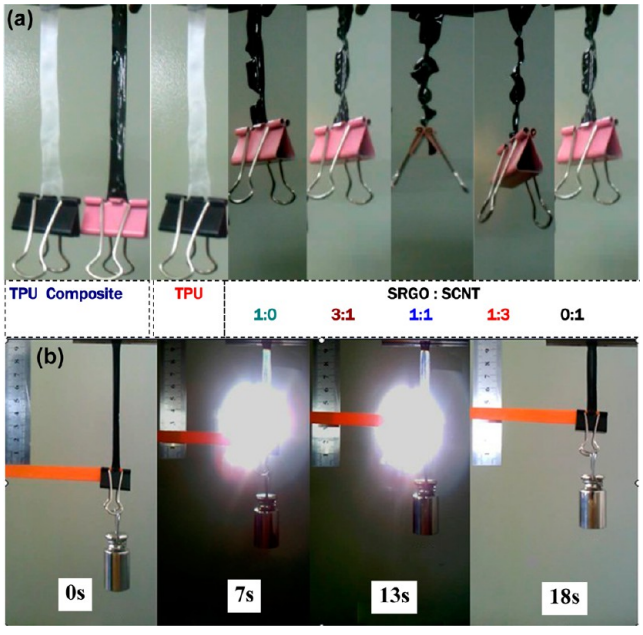

Figure 5. Optical images of the shape recovery of (a) TPU and SRGO/SCNT/TPU composite films with different weight ratios before and after IR irradiation and (b) the stress recovery process of SRGO/SCNT$_{3:1}$/TPU film, which lifts a 107.6 weight 4.7 cm in 18 s remotely actuated by infrared light with an estimated energy density of 0.63 J/g.

radiation, a tremendous shape deformation is utilized for the strain-induced crystallization of soft segments of TPU. Pure TPU is infrared transparent and responds negatively to IR light with no shape changes. In contrast, five SRGO/SCNT/TPU nanocomposite films deform and curl enormously on the exposure to IR source (~30 mW/cm^2) for 10 s. It's known that the shape recovery of TPU is determined by microphase separated heterogeneous structures of soft and hard segments.[40] The crystallinity of soft segments at a low melting

temperature serves as a molecular switch and facilitates the fixation of a strain-induced temporary shape, whereas hard segments are critical for the stabilization of original shape by physical cross-linking. In SRGO/SCNT/TPU nanocomposites, well-dispersed nanofillers absorb IR photons and effectively transfer heat into TPU matrix through phonon transport, leading to an increased temperature of films. IR-triggered recovery arises from the melting of strain-induced physical cross-links of soft segments of TPU at the temperature above T_{soft}. The original shape is stabilized by cross-linked hard segments and SRGO/SCNT nanofillers in TPU based on strong interaction. The strain energy stored in metastable crystalline structures of prestrained TPU can be released in the form of recovery forces driving chains towards original states under IR irradiation.[14,15,18] A typical IR-triggered stress recovery process (Figure 5b) was studied to examine the release of mechanical energy. SRGO/SCNT$_{3:1}$/TPU film lifted a 107.6 g weight up 4.7 cm within 18 s and delivered an energy density of 0.63 J/g, which was almost one-fold higher than that of the previous study.[14]

Generally, the mechanical energy output of shape-memory actuators is determined by the relationship between recoverable stress and strain (shape deformation).[41,42] Thus, mechanical properties (Young's modulus) and the capability for heat transfer absorbed by IR light are important for IR-triggered stress recovery. The reinforcement and enhanced thermal conductivity of SRGO/SCNT/TPU nanocomposites controlled by SRGO:SCNT were shown in Figure 6. Figure 4s

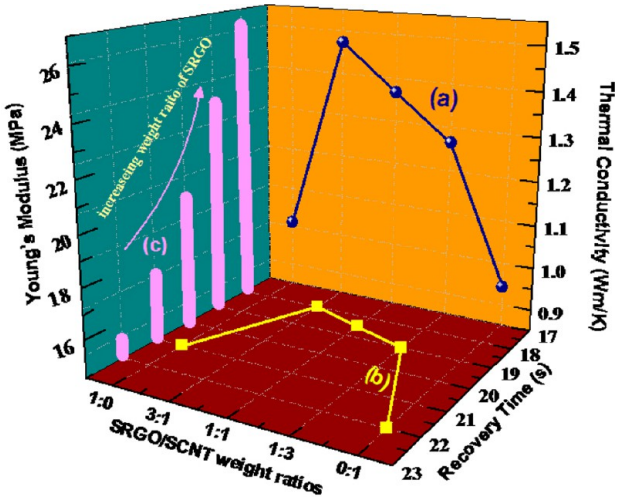

Figure 6. (a) Thermal conductivities, (b) the recovery time, and Young's modulus of SRGO/SCNT/TPU films with SRGO:SCNT of 1:0, 3:1, 1:1, 1:3, and 0:1. Arrows indicates the increasing weight ratio of SRGO in hybrid nanofillers.

in the Supporting Information display representative stress-strain behaviors of SRGO/SCNT/TPU films. Compared with pure TPU (modulus of 12 MPa, not shown), with an increasing ratio of SRGO, nanocomposite films become stronger and stiffer, and SRGO/SCNT$_{3:1}$TPU film performs a Young's modulus up to 23.4 MPa, which is higher than that using other nanofillers except for SRGO/TPU film (26.3 MPa). The strength is comparable or larger than recent studies.[14,16,43−45] High stiffness is crucial for enhanced IR-triggered recovery forces released by strain energy.[18,46] Furthermore, SRGO/SCNT hybrid also leads to higher thermal conductivity (>1.25 W/mK) than that using individual SRGO (1.01 W/mK) or SCNT (0.94 W/mK) nanofiller. Compared with SRGO/SCNT$_{1:1}$/TPU (1.36 W/mK) and SRGO/SCNT$_{1:3}$/TPU film (1.27 W/mK), SRGO/SCNT$_{3:1}$/TPU film shows the maximum thermal conductivity of 1.47 W/mK, which is superior to other TPU composites[16,17,43,47] because of synergistic effect between well-dispersed SRGO and SCNT nanofillers. As shown in Figure 6b, the shape recovery is also accelerated by high thermal conductivity. Thus, the combination of the mechanical reinforcement and high phonon transport can be utilized for high-performance IR-triggered shape recovery.

IR-actuated stress recovery properties of TPU nanocomposites controlled by SRGO:SCNT (1:0, 3:1, 1:1, 1:3 and 0:1) were shown in Figure 7. SRGO/SCNT hybrid

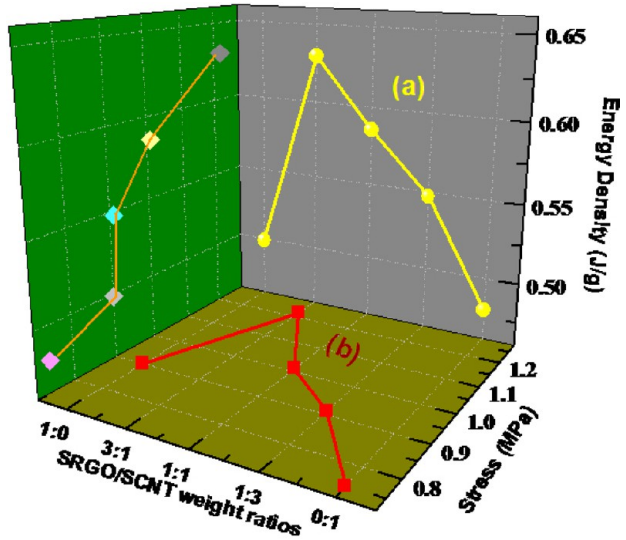

Figure 7. (a) Energy densities and (b) shape recovery forces (stress) of SRGO/SCNT/TPU films with SRGO:SCNT of 1:0, 3:1, 1:1, 1:3, and 0:1. The line with solid circles indicates that the change of energy density and stress controlled by SRGO:SCNT is accordant.

nanofillers result in the shape recovery forces (F_r) higher than 0.9 MPa and energy densities (ω) over 0.55 J/g and, which are better than SRGO/TPU (0.48 J/g and 0.88 MPa) and SCNT/TPU (0.45 J/g, 0.75 MPa). The curve (the line with solid circles in Figure 7) indicates that the changing trend of F_r and ω controlled by SRGO:SCNT was accordant. With the combination of high Young's modulus (23.4 MPa) and high thermal conductivity of 1.47 W//mK, SRGO/SCNT$_{3:1}$/TPU film performs the best IR-triggered shape recovery with F_r of 1.22 MPa and ω up to 0.63 J/g, which are superior to SRGO/SCNT$_{1:1}$/TPU (1.01 MPa, 0.58 J/g) and SRGO/SCNT$_{1:3}$/TPU film (0.91 MPa, 0.55 J/g). Such IR-triggered stress recovery outperforms many polymeric actuators using graphene or CNT nanofillers.[14−16,48,49]

Figure 7 also shows that the stress recovery decreases when SRGO:SCNT is lower than 3:1, which is mainly attributed to low mechanical strength (Figure 6c) and inefficient heat conduction (Figure 6a) affected by excess SCNT in TPU matrix. Previous results indicated that thermal conductivity of polymers filled by graphene/CNT hybrid nanofillers depended on the percolation threshold of 2D graphene,[25,50] and thus when a large amount of SCNT is filled in TPU, disconnected nanotubes not only tend to form several bundles due to the strong attraction but also increase phonon scattering during

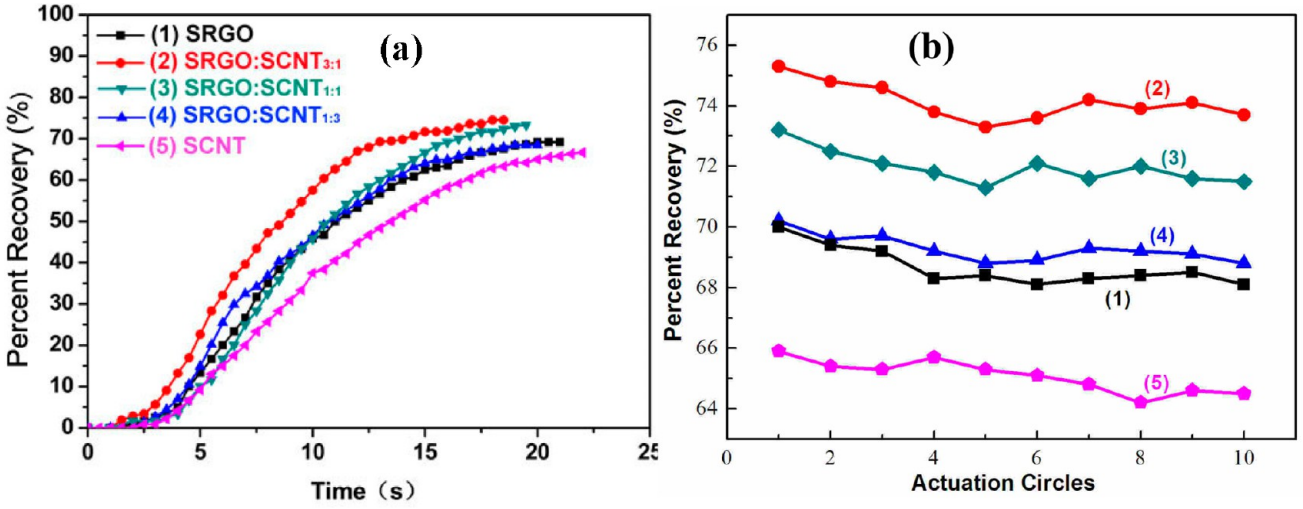

Figure 8. (a) Shape recovery and (b) pencent recovery of (1) SRGO/TPU, (2) SRGO/$SCNT_{3:1}$/TPU, (3) SRGO/$SCNT_{1:1}$/TPU, (4) SRGO/$SCNT_{1:3}$/TPU, and (5) SCNT/TPU film in 10 cycles.

heat conduction,[26] resulting in the decreased thermal conductivity. When individual SRGO nanofiller is incorporated, in spite of high tensile strength, SRGO/TPU film also shows a low IR-triggered stress recovery due to the combining effect of partially limited crystallization soft-segment by strong physical cross-linking, low thermal conductivity and IR absorption. Results indicate that a trade-off between the stiffness and efficient heat transfer of SRGO/$SCNT_{3:1}$/TPU film results in remarkable IR-actuated stress recovery. Further studies on IR-triggered shape recovery of SRGO/SCNT/TPU nanocomposites by optimizing heat transfer and mechanical properties based on synergistic effect between well-dispersed SRGO and SCNT are ongoing.

Figure 8a gives IR-triggered percent recovery of SRGO/SCNT/TPU nanocomposites. Three typical stages are observed in all shape recovery curves acquired from video. At the first stage, polymer nanocomposite film recovered its shape slowly with a low percent recovery due to the conformation hysteresis. Under continuous IR irradiation, an increasing percent recovery at the second stage is attributed to the loss of physical cross-linking of soft segments of TPU at the temperature higher than T_{soft}. The shape recovery becomes slow at the third stage until the balance. As shown in Table 1s in the Supporting Information, SRGO/SCNT/TPU exhibits larger shape recovery and shorter recovery time than that of SRGO/TPU and SCNT/TPU because of the increase in thermal conductivity and mechanical strength. SRGO/$SCNT_{3:1}$/TPU film shows the best shape recovery with the recovery strain up to 75% and the shortest recovery time of 18 s among five films. The corresponding power conversion efficiency (η) is 2.29%. This recovery strain can be increased by utilizing a low-weight load, but it will affect mechanical power output.[42] Despite different percent recoveries, all SRGO/SCNT/TPU films show good cycling stability of IR-actuated stress recovery during 10 cycles (Figure 8b). The percent recovery of SRGO/$SCNT_{3:1}$/TPU, SRGO/$SCNT_{1:1}$/TPU, and SRGO/$SCNT_{1:3}$/TPU fluctuated in the range of 73.5−75.3%, 68.9−70.2%, and 71.6−73.2%, respectively.

4. CONCLUSIONS

3D interconnected SRGO/SCNT hybrids serving as IR absorbers, heat transfer units, and strong nanofillers were integrated into TPU for the fabrication of high-performance IR-triggered actuators. Well-dispersed SRGO/SCNT hybrid with the strong interaction between nanofiller and TPU not only improved the physical cross-linking of soft segments for a large shape deformation but also resulted in the reinforcement and high thermal conductivity. The output stress, energy density and recovery time of IR-triggered actuators were tuned by SRGO:SCNT in TPU matrix. SRGO/$SCNT_{3:1}$/TPU nanocomposite shows the best IR-actuated stress recovery of lifting a 107.6 g weight up 4.7 cm in 18 s. Remarkable IR-actuated recovery delivered a high energy density up to 0.63 J/g and the mechanical stress of 1.2 MPa attributed to high thermal conductivity of 1.473 W/mK and Young's modulus of 23.4 MPa. Such IR-triggered recovery outperforms many optical actuators reported previously.[14−16,48,49] Results indicate that a trade-off between the stiffness and efficient heat transfer controlled by synergistic effect between SRGO and SCNT is critical for high mechanical power output of IR triggered actuators. IR-actuated recovery of SRGO/SCNT/TPU nanocomposites combining high energy density, output forces, and good cycling stability can be further developed for advanced optomechanical systems.

■ ASSOCIATED CONTENT

Supporting Information

TEM images of SRGO and SCNT, FT-IR spectra, absorption spectra, and representative stress−strain behavior of SRGO/SCNT/TPU nanocomposites with different weight ratios. The performance of IR-triggered shape recovery of SRGO/SCNT/TPU nanocomposites including percent recovery, recovery time, and power conversion efficiency. This material is available free of charge via the Internet at http://pubs.acs.org.

■ AUTHOR INFORMATION

Corresponding Author

*E-mail: weifeng@tju.edu.cn. Tel: +86-22-87402059. Fax: +86-22-27404724.

Notes

The authors declare no competing financial interest.

■ ACKNOWLEDGMENTS

This work was financially supported by the National Basic Research Program of China (Grant 2012CB626800 and 2010CB934700), the National Natural Science Foundation of China (Grant 51073115, 51003072, 51173127, and 51273144), and the Research Fund for the Doctoral Program of Higher Education of China (Grant 20110032110067).

■ REFERENCES

(1) Wei, Z. G.; Sandstrom, R.; Miyazaki, S. *J. Mater. Sci.* **1998**, *33*, 3743−3762.
(2) Lendlein, A.; Kelch, S. *Angew. Chem., Int. Ed.* **2002**, *41*, 2034−2057.
(3) Xie, T. *Nature* **2010**, *464*, 267−270.
(4) Ahn, S. K.; Kasi, R. M. *Adv. Funct.Mater.* **2011**, *21*, 4543−4549.
(5) Yu, Z. B.; Zhang, Q. W.; Li, L.; Chen, Q.; Niu, X. F.; Liu, J.; Pei, Q. B. *Adv. Mater.* **2011**, *23*, 664−668.
(6) Cho, J. W.; Kim, J. W.; Jung, Y. C.; Goo, N. S. *Macromol. Rapid Commun.* **2005**, *26*, 412−416.
(7) Razzaq, M. Y.; Behl, M.; Lendlein, A. *Adv. Funct. Mater.* **2012**, *22*, 184−191.
(8) Li, G. Q.; Nettles, D. *Polymer* **2010**, *51*, 755−762.
(9) Koerner, H.; White, T. J.; Tabiryan, N. V.; Bunning, T. J.; Vaia, R. A. *Mater. Today* **2008**, *11*, 34−42.
(10) Hu, J. L.; Zhu, Y.; Huang, H. H.; Lu, J. *Prog. Polym. Sci.* **2012**, *37*, 1720−1763.
(11) Serak, S.; Tabiryan, N.; Vergara, R.; White, T. J.; Vaia, R.; Bunning, T. J. *Soft Matter* **2010**, *6*, 779−783.
(12) Cheng, F.; Yin, R.; Zhang, Y.; Yen, C. C.; Yu, Y. *Soft Matter* **2010**, *6*, 3447−3449.
(13) Miaudet, P.; Derre, A.; Maugey, M.; Zakri, C.; Piccione, P. M.; Inoubli, R.; Poulin, P. *Science* **2007**, *318*, 1294−1296.
(14) Liang, J. J.; Xu, Y. F.; Huang, Y.; Zhang, L.; Wang, Y.; Ma, Y. F.; Li, F. F.; Guo, T. Y.; Chen, Y. S. *J. Phys. Chem. C* **2009**, *113*, 9921−9927.
(15) Koerner, H.; Price, G.; Pearce, N. A.; Alexander, M.; Vaia, R. A. *Nat. Mater.* **2004**, *3*, 115−120.
(16) Jung, Y. C.; Kim, H. H.; Kim, Y. A.; Kim, J. H.; Cho, J. W.; Endo, M.; Dresselhaus, M. S. *Macromolecules* **2010**, *43*, 6106−6112.
(17) Jung, Y. C.; Kim, J. H.; Hayashi, T.; Kim, Y. A.; Endo, M.; Terrones, M.; Dresselhaus, M. S. *Macromol. Rapid Commun.* **2012**, *33*, 628−634.
(18) Leng, J. S.; Wu, X. L.; Liu, Y. J. *J. Appl. Polym. Sci.* **2009**, *114*, 2455−2460.
(19) Yadav, S. K.; Cho, J. K. *Appl. Surf. Sci.* **2013**, *266*, 360−367.
(20) Sahoo, N. G.; Rana, S.; Cho, J. W.; Li, L.; Chan, S. H. *Prog. Polym. Sci.* **2010**, *35*, 837−867.
(21) Balandin, A. A. *Nat. Mater.* **2011**, *10*, 569−581.
(22) Dreyer, D. R.; Park, S.; Bielawski, C. W.; Ruoff, R. *Chem. Soc. Rev.* **2010**, *39*, 228−240.
(23) Huang, X. Y.; Zhi, C. Y.; Jiang, P. K. *J. Phys. Chem. C* **2012**, *116*, 23812−23820.
(24) Aravind, S. S. J.; Ramaprabhu, S. *RSC Adv.* **2013**, *3*, 4199−4206.
(25) Chu, K.; Li, W. S.; Jia, C. C.; Tang, F. L. *Appl. Phys. Lett.* **2012**, *10*, 211903.
(26) Im, H.; Kim, J. *Carbon* **2012**, *50*, 5429−5440.
(27) Shin, M. K.; Lee, B.; Kim, S. H.; Lee, J. A.; Spinks, G. M.; Gambhir, S.; Wallace, G. G.; Kozlov, M. E.; Baughman, R. H.; Kim, S. J. *Nat. Commun.* **2012**, *3*, 650.
(28) Feng, Y. Y.; Zhang, H. B.; Hou, Y.; McNicholas, T. P.; Yuan, D. N.; Yang, S. W.; Ding, L.; Feng, W.; Liu, J. *ACS Nano* **2008**, *2*, 1634−1638.
(29) Si, Y. C.; Samulski, E. T. *Nano Lett.* **2008**, *8*, 1679−1682.
(30) Peng, L. W.; Feng, Y. Y.; Lv, P.; Lei, D.; Shen, Y. T.; Li, Y.; Feng, W. *J. Phys. Chem. C* **2012**, *116*, 4970−4978.
(31) Auad, M. L.; Contons, V. S.; Nutt, S.; Aranguren, M. I.; Marcovich, N. E. *Polym. Int.* **2008**, *57*, 651−659.
(32) Kim, H.; Abdala, A. A.; Macosko, C. W. *Macromolecules* **2010**, *43*, 6515−6530.
(33) Ha, H. W.; Choudury, A.; Kamal, T.; Kim, D. H.; Park, S. Y. *ACS Appl. Mater. Interfaces* **2012**, *4*, 4623−4630.
(34) Acik, M.; Lee, G.; Mattevi, C.; Chhowalla, M.; Cho, K.; Chabal, Y. J. *Nat. Mater.* **2010**, *9*, 840−845.
(35) Acik, M.; Lee, G.; Mattevi, C.; Pirkle, A.; Wallace, R. M.; Chhowalla, M.; Cho, K.; Chabal, Y. *J. Phys. Chem. C* **2011**, *115*, 19761−19781.
(36) Robinson, J. T.; Tabakman, S. M.; Liang, Y. Y.; Wang, H. L.; Casalongue, H. S.; Vinh, D.; Dai, H. J. *J. Am. Soc. Chem.* **2011**, *133*, 6825−6831.
(37) Cheng, S.; Chen, X.; Hsuan, Y. G.; Li, C. Y. *Macromolecules* **2012**, *45*, 993−1000.
(38) Barick, A. K.; Tripathy, D. K. *Mater. Sci. Eng., B* **2011**, *176*, 1435−1447.
(39) Lee, H. F.; Yu, H. H. *Soft Matter* **2011**, *7*, 3801−3807.
(40) Lee, B. S.; Chun, B. C.; Chung, Y. C.; Sul, K. I.; Cho, J. W. *Macromolecules* **2001**, *34*, 6431−6437.
(41) Rana, S.; Cho, J. W.; Tan, L. P. *RSC Adv.* **2013**, *3*, 13796−13803.
(42) Rapp, S.; Baier, H. *Smart Mater. Struct.* **2010**, *19*, 045018.
(43) Yadav, S. K.; Yoo, H. J.; Cho, J. W. *J. Polym. Sci., Part B: Polym. Phys.* **2012**, *51*, 39−47.
(44) Yoon, S. H.; Park, J. H.; Kim, E. Y.; Kim, B. K. *Colloid Polym. Sci.* **2011**, *289*, 1809−1814.
(45) Cai, D. Y.; Jin, J.; Yusoh, K.; Rehman, R.; Song, M. *Compos. Sci. Technol.* **2012**, *72*, 702−707.
(46) Gall, K.; Dunn, M. L.; Liu, Y. P. *Appl. Phys. Lett.* **2004**, *85*, 290−292.
(47) Cai, D.; Song, M. *Carbon* **2008**, *46*, 2107−2112.
(48) Yang, L. Q.; Setyowati, K.; Li, A.; Gong, S. Q.; Chen, J. *Adv. Mater.* **2008**, *20*, 2271−2275.
(49) Choi, J. T.; Dao, T. D.; Oh, K. M.; Lee, H.; Jeong, H. M.; Kim, B. K. *Smart Mater. Struct.* **2012**, *21*, 075017.
(50) Stankovich, S.; Dikin, D. A.; Dommett, G. H. B.; Kohlhaas, K. M.; Zimney, E. J.; Stach, E. A.; Piner, R. D.; Nguyen, S. T.; Ruoff, R. S. *Nature* **2006**, *442*, 282−286.